Met. Mater. Int., Vol. 19, No. 1 (2013), pp. 19~25
doi: 10.1007/s12540-013-1004-7

Through-Thickness SCC Susceptibility of 2024-T351 and 7050-T7451 Extrudates in 3.5% NaCl Solution

Youngju Kim[1], Jaeki Kwon[1], Yooin Jeong[2], Namsub Woo[1], and Sangshik Kim[3,*]

[1]Mineral Resources Research Division, Korea Institute of Geoscience & Mineral Resources, Daejeon 305-350, Korea
[2]Airframe Design Section Research & Development Division, Korea aerospace industries, LTD. Sacheon 664-710, Korea
[3]Department of Materials Science and Engineering, ReCAPT, Gyeongsang National University, Chinju 660-701, Korea

(received date: 27 December 2011 / accepted date: 12 March 2012)

The through-thickness stress corrosion cracking (SCC) behaviors of thick 2024-T351 and 7050-T7451 extrudates in 3.5% NaCl solution were studied at both anodic and cathodic applied potentials using a slow strain rate test method. The SCC susceptibilities of 2024-T351 extrudate tended to change in the through-thickness direction, with the lowest susceptibility for the surface specimen. 7050-T7451 specimens, on the other hand, did not show a notable change in the through-thickness SCC susceptibility. The fractographic analysis suggested that the grain boundary played an important role in determining the SCC susceptibility. The SCC process of each alloy was discussed based on the microscopic and fractographic examinations.

Key words: stress corrosion cracking, alloy, extrusion, strain rate, tensile test

1. INTRODUCTION

Age-hardenable 2xxx and 7xxx aluminum alloys are susceptible to stress corrosion cracking (SCC) which has been the subject of extensive research activities particularly in the aerospace industry [1-5]. When high-strength aluminum alloys are exposed to an SCC-causing environment, pits are formed, which become deeper and start to be connected by a network of intergranular corrosion paths [6,7]. Hydrogen is then produced by these anodic dissolution type of surface corrosion reactions and part of it is absorbed in atomic form into the material, causing hydrogen embrittlement [8,9]. For example, in Al 2024 (Al-Cu-Mg) in an SCC-causing environment, stable pit initiation occurs at a cluster of particles and the intergranular corrosion cracking (IGC) inter-connects these corrosion pits [10]. The preferential contribution of anodic dissolution and hydrogen embrittlement for an SCC process may vary with different alloy/environment systems [11]. Hydrogen embrittlement is known to be a controlling SCC mechanism for Al 7050 (Al-Zn-Mg-Cu) in a wet air environment, with a tendency of corrosion attacking on the grain interior. For Al 2024, on the other hand, the crack growth tends to follow a fine network of grain boundaries [12-14].

A complex aerospace part is often produced by mechanical machining from thick plate, and the mid-section of such plate is exposed to an SCC-causing environment [15]. Since grain boundaries play an important role in the SCC process, the SCC susceptibility of thick plate may vary with varying grain characteristics in the through-thickness direction. It is therefore practically important to understand the SCC behavior of high-strength Al alloys in the through-thickness direction. It has been suggested that the aspect ratio of grain and the precipitates along grain boundaries are the major controlling factors on the through-thickness SCC behavior of high-strength Al alloys [16,17]. Different SCC responses are often observed for certain grain directions with different alloy systems, such that the stress corrosion crack in Al 2024 grows along the longitudinal (L) direction at about the same rate that it grows along the transverse (T) direction, while it grows fastest in Al 7050 along the T direction [18,19]. Therefore the through-thickness SCC behaviors of these two, the most widely used Al alloys in aircraft structures, would be different from each other. The preferential contribution between anodic dissolution and hydrogen embrittlement may affect the through-thickness SCC response differently in different alloy systems. Despite the practical significance, only limited studies are available on the through-thickness SCC behavior of high-strength aluminum alloy [17]. In this study, the through-

*Corresponding author: sang@gnu.ac.kr

thickness SCC behaviors of thick 2024-T351 and 7050-T7451 extrudates in 3.5% NaCl solution were examined at both anodic and cathodic applied potentials using a slow strain rate test (SSRT) method. The SEM (scanning electron microscope) fractographic analyses were conducted on the slow strain rate tested specimens to understand the SCC process of initiation and propagation for both alloys. The different SCC responses with different grain structures in the through-thickness direction for 2024-T351 and 7050-T7451 were discussed.

2. EXPERIMENTAL PROCEDURES

To study the through-thickness SCC behavior, two commercial aluminum alloys of 76 mm thick 2024-T351 and 96 mm thick 7050-T7451 extrudates were used. The smooth tensile specimens with a gauge length of 20 mm and a diameter of 4 mm were prepared from each extrudate with the grain direction parallel to the longitudinal (L) direction at surface, quarter-section (T/4) and mid-section (T/2). The chemical compositions and tensile properties are given in Tables 1 and 2. The tensile properties in Table 2 were measured at a nominal strain rate of 1×10^{-3}/sec. A slow strain rate test (SSRT) method was utilized to evaluate the through-thickness SCC susceptibility of 2024-T351 and 7050-T7451 in 3.5% NaCl solution. The SSRT was carried out in an aqueous 3.5% NaCl solution on an R&B model T07-025 constant extension rate test (CERT) machine in accordance with ASTM G129 [20]. The OCP (open circuit potential) was measured on both alloys in 3.5% NaCl solution using a PAR model Versa Stat II potentiostat in accordance with ASTM G5 [21]. Based on the measured OCP values for each alloy, as shown in Fig. 1, the SSRT was conducted at an anodic (50 mV vs. SCE above OCP) and a cathodic (50 mV vs. SCE below OCP) at a strain rate of 5×10^{-7}/sec in 3.5% NaCl solution. A quantitative indication of SCC severity was expressed by a percent decrease in tensile elongation in 3.5% NaCl solution over those in an air environment. The rationale for using the percent decrease in tensile elongation in 3.5% NaCl solution, over those in air, as a SCC susceptibility for high-strength aluminum alloy is described elsewhere [2,22-24]. For the micrographic observation, the specimens were polished and etched by using a Graff/Sargent's reagent (0.5 ml HF + 15.5 ml HNO_3 + 84 mL H_2O + 3.0 g CrO_3). The SEM micrographic and fractographic analyses were conducted on selected specimens to identify the mode of fracture and the SCC mechanisms.

Table 2. Tensile properties of 2024-T351 and 7050-T7451 with different grain directions at a nominal strain rate of 1×10^{-3}/sec

Material	Grain direction	YS (MPa)	UTS (MPa)	Tensile elongation (%)
2024-T351	Surface	315	409	8.2
	T/4	324	425	9.7
	T/2	325	439	11.7
7050-T7451	Surface	476	530	15
	T/4	480	529	13
	T/2	481	532	13

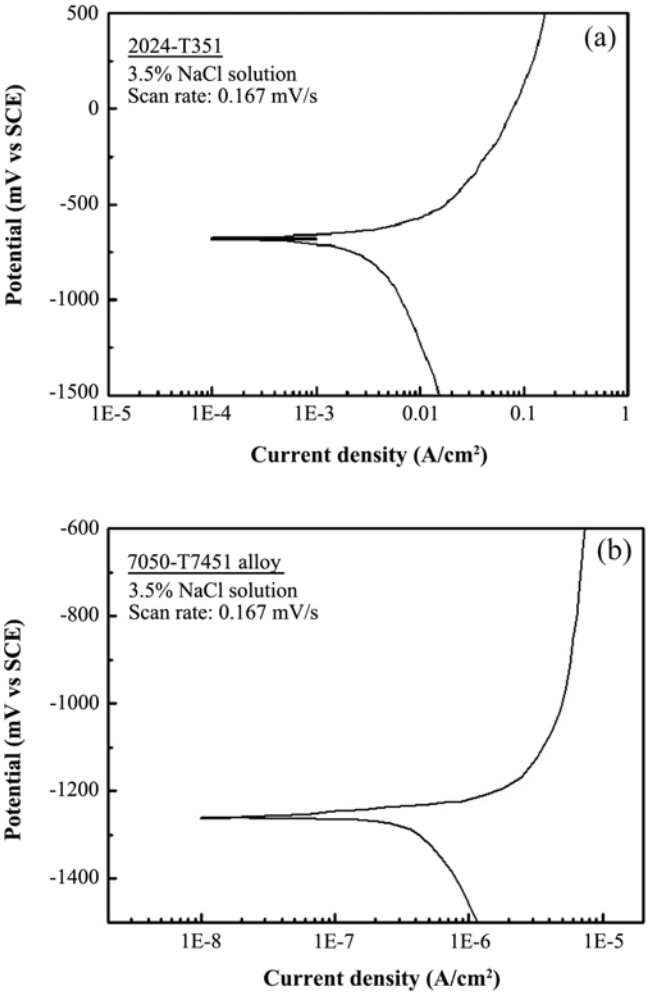

Fig. 1. Open circuit potential values measured for (a) 2024-T351 and (b) 7050-T7451 in 3.5% NaCl solution.

Table 1. Chemical composition (wt%) of 2024-T351 and 7050-T7451

Material	Cu	Mg	Zn	Fe	Si	Mn	Cr	Others	Al
2024-T351	3.8-4.9	1.2-1.8	0.25	~0.50	~0.50	0.3-0.9	0.1	< 0.20	bal.
7050-T7451	2.0-2.6	1.9-2.6	5.7-6.7	~0.15	~0.12	~1.0	~0.04	<0.41	bal.

3. RESULTS AND DISCUSSION

Figures 2 and 3 show (a) the 3-D optical micrographs of 2024-T351 (Fig. 2) and 7050-T7451 (Fig. 3) and the microstructures documented at (b) surface, (c) T/4 and (d) T/2 on the S-L plane. Partially recrystallized, pan-cake shaped grain structures were observed for both 2024-T351 and 7050-T7451 specimens. The grain shape of 2024-T351 extrudate tended to vary in the through-thickness direction, such that the degree of recrystallization and the average aspect ratio increased in the depth direction. For the 7050-T7451 specimen, a number of fine equiaxed grains and large unrecrystallized grains were observed. The change in grain structure of 7050-T7451 in the through-thickness direction was not as notable as that of 2024-T351.

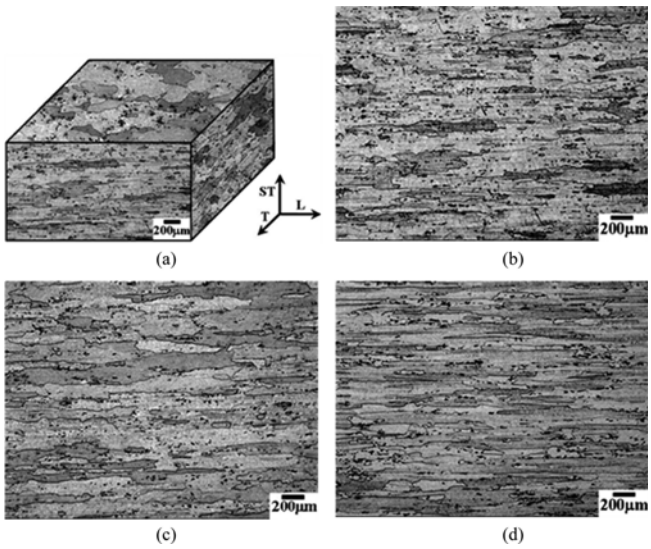

Fig. 2. Optical micrographs of 76 mm thick 2024-T351 extrudate (a) in 3-D view and those documented at (b) surface, (c) T/4 and (d) T/2 on the S-L plane.

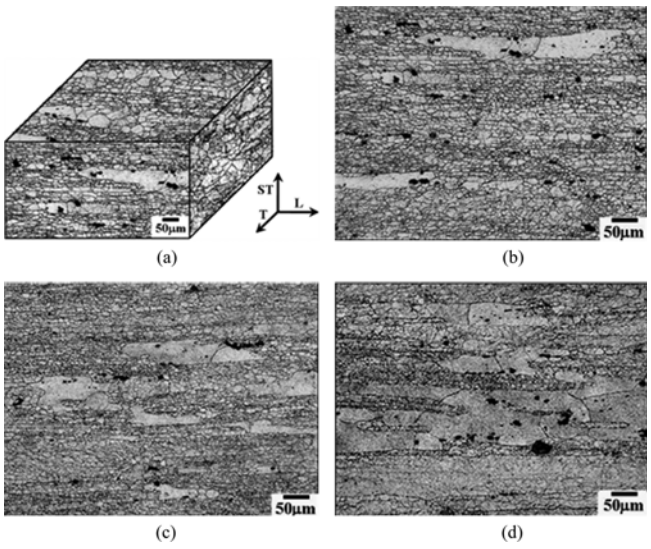

Fig. 3. The optical micrographs of 96 mm thick 7050-T7451 extrudate (a) in 3-D view and those documented at (b) surface, (c) T/4 and (d) T/2 on the S-L plane.

Tables 3 and 4 show the varying SCC susceptibilities of 2024-T351 (Table 3) and 7050-T7451 (Table 4) specimens in the through-thickness direction. All the SSRTs were conducted at a strain rate of 5×10^{-7}/sec in air and 3.5% NaCl solution either at an applied potential of 50 mV vs. SCE above (anodic applied potential) and below (cathodic applied potential) the OCV values, and the SCC susceptibility was represented by the percent reduction in tensile elongation in 3.5% NaCl, over it in an air environment. It was previously demonstrated that the SCC susceptibility of the present alloys was best represented by the percent reduction, while the changes in UTS, YS and time to fracture were not consistent with varying testing variables [4]. The Tables 3 and 4 demonstrate that the through-thickness SCC susceptibilities tend to change for the 2024-T351 specimens but not for the 7050-T7451 specimens at both applied potentials. The 2024-T351 specimens prepared from the surface area of extrudate, for example, showed lower SCC susceptibility compared to those for the T/4 and T/2 specimens at both cathodic and anodic applied potentials. The SCC susceptibilities of 2024-T351 specimens prepared from T/4 and T/2 were similar with each other, but higher than that for the surface specimens. The SCC susceptibilities for the 7050-T7451 specimens were substantially lower than those for the 2024-T351 specimens at both applied potentials; such a trend has often been reported in the literature [2]. The through-thickness SCC susceptibilities of the 7050-T7451 specimens did not show any notable change in the through-thickness direction.

Figures 4 and 5 represent the SEM fractographs of the 2024-T351 specimens prepared from (a) surface, (b) T/4 and (c) T/2 at an anodic potential of –632 mV vs. SCE (Fig. 4) and a cathodic potential of –732 mV vs. SCE (Fig. 5). With high-strength aluminum alloys exposed to an SCC-causing environment, pits are formed and start to be connected by a network of intergranular corrosion paths [12,18]. This intergranular corrosion cracking (IGC) is accelerated by an anodic applied potential during SSRT [25]. Hydrogen is then produced by the surface corrosion reactions and part of it is absorbed in atomic form into the material, causing hydrogen embrittlement [6,26-27]. At an anodic applied potential of -632 mV vs. SCE in 3.5% NaCl solution, the IGC mode was dominant for all the SSRTed 2024-T351 specimens. However, the depth of this IGC zone changed in the through-thickness direction. The IGC zone was approximately 1.0 mm for the surface compared to 1.2–1.3 mm for the T/4 and T/2, demonstrating a greater resistance to SCC for the surface than the mid-section. At a cathodic applied potential, on the other hand, semi-circular shaped cleavage facets were observed in the SCC initiation areas along the circumference. The number of these cleavage facets on the fracture surface was

Table 3. SSRT results for the 2024-T351 specimens with the grain direction of L in 3.5% NaCl solution at a nominal strain rate of 5×10^{-7}/sec

Applied potential (mV vs. SCE)	Location	Environments	YS (MPa)	UTS (MPa)	Tensile elongation (%)	
						% Reduction*
–632	Surface	Air	376	475	21	52
		NaCl	210	215	10	
	T/4	Air	388	496	19	82
		NaCl	211	212	3.5	
	T/2	Air	395	507	17	89
		NaCl	289	290	2	
–732	Surface	Air	374	477	24	17
		NaCl	376	473	20	
	T/4	Air	388	496	19	37
		NaCl	344	415	12	
	T/2	Air	395	507	17	35
		NaCl	385	468	11	

*% Reduction = $TE_{air}–TE_{3.5NaCl}/TE_{air}$

Table 4. SSRT results for the 7050-T7451 specimens with the grain direction of L in 3.5% NaCl solution at a nominal strain rate of 5×10^{-7}/sec

Applied potential (mV vs. SCE)	Location	Environments	YS (MPa)	UTS (MPa)	Tensile elongation (%)	
						% Reduction*
–1225	Surface	Air	493	517	16	25
		NaCl	482	503	12	
	T/4	Air	469	502	12	20
		NaCl	484	512	9.6	
	T/2	Air	480	514	11	22
		NaCl	438	467	8.7	
–1325	Surface	Air	493	517	16	–6
		NaCl	515	523	17	
	T/4	Air	469	502	12	–5
		NaCl	495	522	13	
	T/2	Air	480	514	11	–6
		NaCl	483	512	11.7	

*% Reduction = $TE_{air}–TE_{3.5NaCl}/TE_{air}$

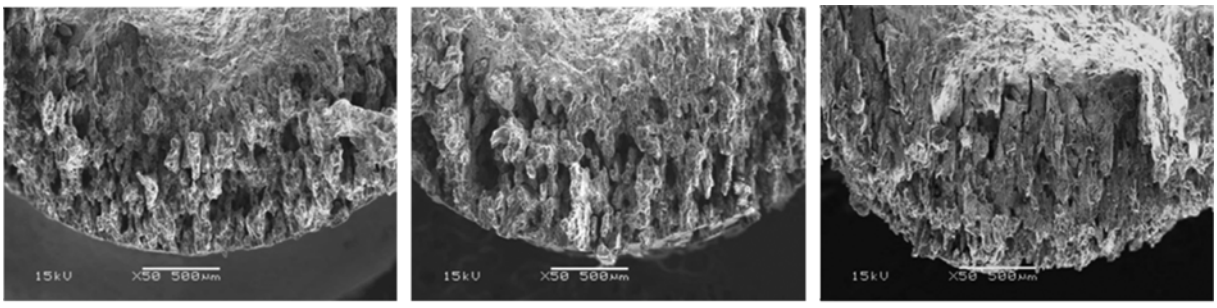

(a) (b) (c)

Fig. 4. The SEM fractographs of the SSRTed 2024-T351 specimens prepared from (a) surface, (b) T/4 and (c) T/2 at an anodic potential of –632 mV vs. SCE.

less, while the size was much greater, for the SSRTed 2024-T351 specimens prepared from surface, than those from T/2 and T/4. The formation of these cleavage facets has been known to be related to hydrogen embrittlement during SCC process, as mentioned previously [25]. The present fractographic examination in Fig. 4 suggested that the 2024-T351 specimens from T/2 and T/4 provided more SCC initiation sites than those from surface. More stress corrosion cracks formed on the surface would obviously increase the SCC susceptibility.

Figures 6 and 7 show the SEM fractographs of the SSRTed 7050-T7451 specimens prepared from (a) surface, (b) T/4

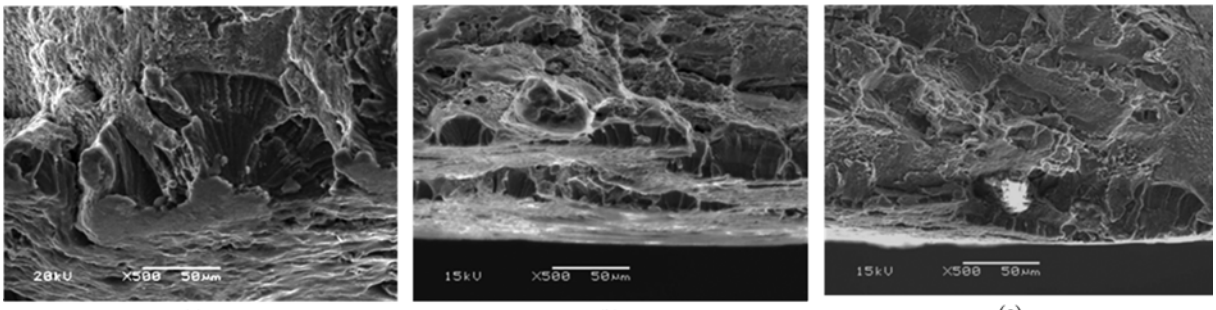

Fig. 5. The SEM fractographs of the SSRTed 2024-T351 specimens prepared from (a) surface, (b) T/4, and (c) T/2 at a cathodic potential of −732 mV vs. SCE.

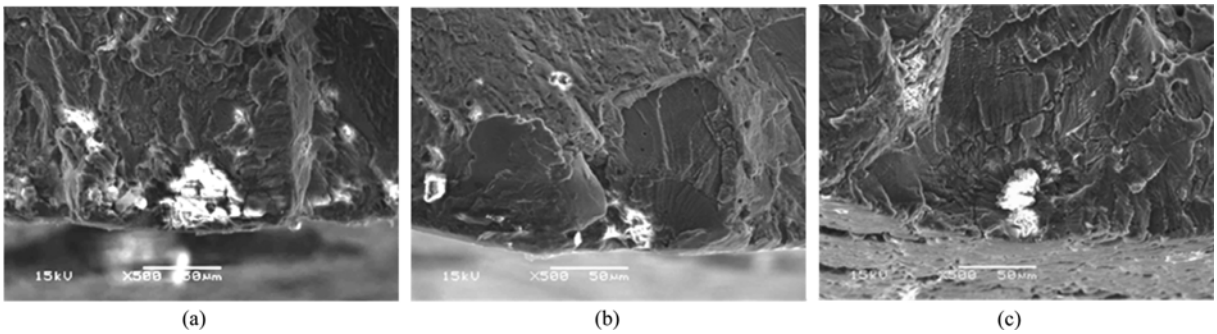

Fig. 6. The SEM fractographs of the SSRTed 7050-T7451 specimens prepared from (a) surface, (b) T/4, and (c) T/2 at an anodic potential of −1225 mV vs. SCE.

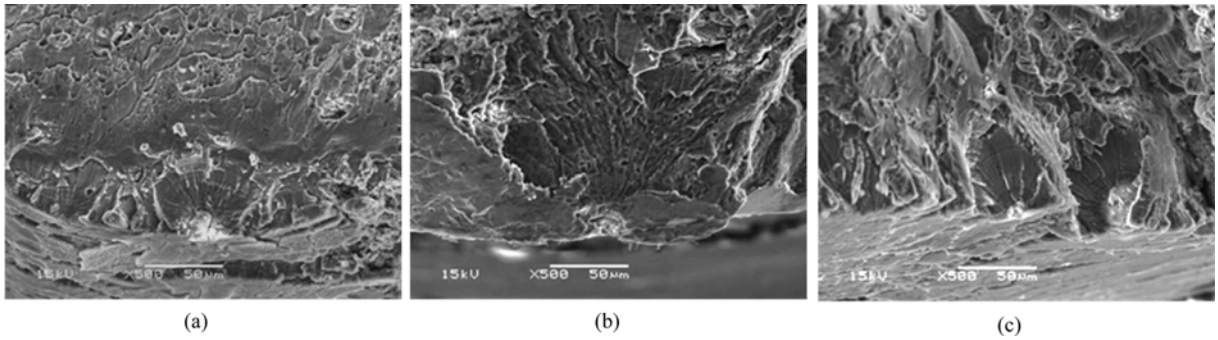

Fig. 7. The SEM fractographs of the SSRTed 7050-T7451 specimens prepared from (a) surface, (b) T/4, and (c) T/2 at a cathodic potential of −1325 mV vs. SCE.

and (c) T/2 at an anodic potential of −1225 mV vs. SCE (Fig. 6) and a cathodic potential of −1325 mV vs. SCE (Fig. 7). It was demonstrated that semi-circular cleavage facets were developed from corrosion pits formed at constituent particle for the SSRTed 7050-T7451 specimens at both applied potentials, with the formation of corrosion pits more accelerated at an anodic applied potential. Unlike the 2024-T351 specimens, no fractographic change was noted for the SSRTed 7050-T7451 specimens in the through-thickness direction.

There are a number of studies that suggest corrosion pits are formed at the cluster of constituent particles, such as Al-Cu-Fe-Mn particles for 2024-T351 and Al7CuFe and Al2CuMg particles for 7050-T7451, in a chloride environment, and that these pits serve as initiation points for SCC [28-30]. Figures 4 and 5 suggest that the corrosion pits in the SSRTed 2024-T351 specimens are networked by an intergranular corrosion cracking from the early stage of SCC process. Previously, Kamoustsi and co-workers have proposed that the pit-to-pit interactions by a network of intergranular corrosion paths in Al 2024 alloy leads to pit clustering and coalescence [6]. From that point, corrosion pits do not penetrate deeper, but spread beneath the surface instead. They also proposed that the hydrogen front advances as corrosion proceeds, and the quasi-cleavage zone is formed between the intergranular corrosion zone and the ductile corrosion-unaffected zone [8].

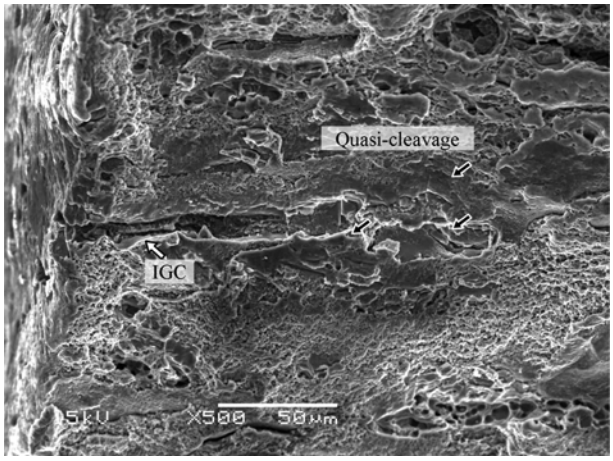

Fig. 8. The networking of corrosion pits by the IGC observed along with a small area of quasi-cleavage fracture at a cathodic applied potential −732 mV vs. SCE for the SSRTed 2024-T351.

For the SSRTed 2024-T351 specimens in this study, a similar networking of corrosion pits by IGC was observed along with a small area of quasi-cleavage fracture at a cathodic applied potential (Fig. 8). Unlike 2024-T351, the corrosion in 7050-T7451 tends to attack the grain interior, rather than the grain boundary, and hydrogen embrittlement (HE) has been proposed to play an important role for such a transgranular cleavage type of SCC propagation.

4. CONCLUSIONS

The through-thickness SCC behaviors of thick 2024-T351 and 7050-T7451 extrudates in 3.5% NaCl solution were examined at both anodic and cathodic applied potentials using a SSRT method, and the following conclusions were drawn.

(1) The SCC susceptibilities of 76 mm thick 2024-T351 extrudate tended to change in the through-thickness direction. The SCC susceptibility was lower for the specimens prepared from the surface of extrudate than those for the specimens from T/4 and T/2 at both cathodic and anodic applied potentials, while both T/4 and T/2 specimens showed similar SCC susceptibilities.

(2) The grain shape of 2024-T351 extrudate varied in the through-thickness direction, such that the degree of recrystallization and the average aspect ratio increased in the depth direction. The fractographic analysis showed that the increase in grain boundary area in the mid-section of extrudate provided more initiation sites for SCC in 3.5% NaCl solution at both anodic and cathodic applied potentials.

(3) The grain structure of 96 mm thick 7050-T7451 extrudate did not change significantly in the through-thickness direction and the change in through-thickness SCC susceptibility was negligible in 3.5% NaCl solution at both anodic and cathodic applied potentials.

ACKNOWLEDGMENTS

This work was supported by the Engineering Research Center Program through the National Research Foundation of Korea (NRF) funded by the Ministry of Education, Science and Technology (2012-0030801). This research was also supported by the Development of Drill Riser System Project (12-9220) and the Basic Research Project "development of optimum technologies of exploration geophysics and mining for the ore deposit targeting" of the KIGAM funded by the Ministry of Knowledge Economy of Korea.

REFERENCES

1. M. O. Speidel, *Met. Trans. A* **6**, 631 (1975).
2. R. P. Gangloff and S. S. Kim, *Environment Enhanced Fatigue Crack Propagation in Metal: Inputs to Fracture Mechanics Life Prediction Model*, NASA Contractor report 191538 (1993).
3. W. K. Jang, S. S. Kim, and K. S. Shin, *Metall. Mater. Trans. A* **33**, 1755 (2002).
4. H. Lee, Y. J. Kim, Y. I. Jeong, and S. S. Kim, *Corros. Sci.* **55**, 10 (2012).
5. Y. L. Choi, R. S. Kalubarme, H. J. Jang, and C. J. Park, *Korean J. Met. Mater.* **49**, 839 (2011).
6. H. Kamoutsi, G. N. Haidemenopoulos, V. Bontozoglou, and S. Pantelakis, *Corros. Sci.* **48**, 1209 (2006).
7. W. Zhang and G. S. Frankel, Electrochem. *Solid. St.* **3**, 268 (2000).
8. P. Leblanc and G. S. Frankel, Electrochem. *Solid. St.* **149**, B239 (2002).
9. M. Büchler, T. Watari, and W. H. Smyrl, *Corros. Sci.* **42**, 1661 (2000).
10. C. Blanc and G. Mankowski, *Corros. Sci.* **40**, 411 (1998).
11. X. Zhang, Z. Sun, Z. Tang, M. Liu, and B. Li, *Proc. Sec. Int. Conf. on Environment-Induced Cracking of Metals (EICM-2)* (eds. S. A. Shipilov, R. H. Jones, J. M. Olive, R. B. Rebak), pp. 351, Elsevier, Amsterdam, Netherlands (2008).
12. W. Zhang and G. S. Frankel, *Electrochim. Acta* **48**, 1193 (2003).
13. N. Birbilis, M. K. Cavanaugh, and R. G. Buchheit, *Corros. Sci.* **48**, 4202 (2006).
14. T. C. Tasi and T. H. Chuang, *Mater. Sci. Eng. A* **225**, 135 (1997).
15. Q. C. Wang, L. T. Wang, and W. Peng, *Mater. Sci. Forum* **490-491**, 97 (2005).
16. M. Posada, L. E. Murr, C. S. Niou, D. Roberson, D. Little, R. Arrowood, and D. George, *Mater. Charact.* **38**, 259 (1997).
17. M. J. Robinson and N. C. Jackson, *Corros. Sci.* **41**, 1013 (1999).
18. S. P. Knight, M. Salagaras, A. M. Wythe, F. De Carlo, A. J. Davenport, and A. R. Trueman, *Corros. Sci.* **52**, 3855 (2010).
19. R. C. Dorward and T. R. Pritchett, *Mater. Design* **9**, 63

(1988).
20. ASTM G129, Standard Practice for Slow Strain Rate Testing to Evaluate the Susceptibility of Metallic Materials to Environmentally Assisted Cracking (2000).
21. ASTM G5, Standard Reference Test Method for Making Potentiostatic and Potentiodynamic Anodic Polarization Measurements (1994).
22. H. J. Lee, Y. J. Kim, Y. I. Jeong, and S. S. Kim, *Corros. Sci.* **55**, 10 (2012).
23. F. Zeides and I. Roman, *Mater. Sci. Eng. A* **125**, 21 (1990).
24. W. K. Jang, S. S. Kim, and K. S. Shin, *Scripta Mater.* **40**, 503 (1999).
25. R. Braun, *Mater. Wiss. Werkst.* **38**, 674 (2007).
26. D. E. Azofeifa, N. Clark, A. Amador, and A. Saenz, *Thin Solid Films* **300**, 295 (1997).
27. H. Z. Wang, D. Y. C. Leung, M. K. H. Leung, and M. Ni, *Renew. Sust. Energ. Rev.* **13**, 845 (2009).
28. P. Campestrini, E. P. M. Westing. H. W. Rooijen, and J. H. W. Wit, *Corros. Sci.* **42**, 1853 (2000).
29. A. Hughes, T. H. Muster, A. Boag, A. M. Glenn, C. Luo, X. Zhou, G. E. Thompson, and D. McCulloch, *Corros. Sci.* **52**, 665 (2010).
30. P. C. King, I. S. Cole, P. A. Corrigan, A. E. Hughes, and T. H. Muster, *Corros. Sci.* **53**, 1086 (2011).